Eur. Phys. J. B **27**, 473–481 (2002)
DOI: 10.1140/epjb/e2002-00180-3

THE EUROPEAN PHYSICAL JOURNAL B

Magnetism and phase separation in the ground state of the Hubbard model

R. Zitzler[1], Th. Pruschke[2,a], and R. Bulla[2]

[1] Institut für Theoretische Physik I, Universität Regensburg, 93040 Regensburg, Germany
[2] Theoretische Physik III, Elektronische Korrelationen und Magnetismus, Institut für Physik, Universität Augsburg, 86135 Augsburg, Germany

Received 9 January 2002
Published online 25 June 2002 –

Abstract. We discuss the ground state magnetic phase diagram of the Hubbard model off half filling within the dynamical mean-field theory. The effective single-impurity Anderson model is solved by Wilson's numerical renormalization group calculations, adapted to symmetry broken phases. We find a phase separated, antiferromagnetic state up to a critical doping for small and intermediate values of U, but could not stabilize a Néel state for large U and finite doping. At very large U, the phase diagram exhibits an island with a ferromagnetic ground state. Spectral properties in the ordered phases are discussed.

PACS. 71.27.+a Strongly correlated electron systems – 71.30.+h Metal-insulator transitions and other electronic transitions – 74.25.Jb Electronic structure

1 Introduction

Originally proposed for the description of ferromagnetism in transition metals, the Hubbard model [1]

$$H = \sum_{i,j} \sum_{\sigma} t_{ij} c^{\dagger}_{i\sigma} c_{j\sigma} + U \sum_{i} n_{i\uparrow} n_{i\downarrow} \qquad (1)$$

is the simplest model to describe the interplay between delocalization or band formation in solids and the local Coulomb correlations. Despite its simplicity, the phase diagram of the Hubbard model (1) reveals a surprising richness. One finds Mott-Hubbard type metal-insulator transitions [2], antiferromagnetism [3], ferromagnetism [4] and incommensurate magnetic phases [5]. More recently, the Hubbard model has also become one of the most promising candidates to describe the low-energy properties and possibly the superconductivity in the high-T_c cuprates [6].

The Hubbard model at half filling $\langle n \rangle = 1$ has been investigated thoroughly using various approximate and exact techniques [7,8] and its properties are understood to a large extent. Off half filling, the model is well understood for $d = 1$ but the situation is less clear in dimensions $d > 1$. Basically the only rigorous result is due to Nagaoka [9], who proved that a ferromagnetic ground state is possible under certain conditions.

The introduction of the limit $D \to \infty$ [10–12] in principle allows to solve models like the Hubbard model exactly without loosing the competition between kinetic energy and local Coulomb repulsion [13]. This surprising insight has subsequently triggered a large amount of investigations of the infinite dimensional Hubbard model [13]. In addition, $D \to \infty$ turned out to be a reasonable starting point for weak-coupling expansions [14,15]. Within this approach, in addition to the expected magnetic order for a bipartite lattice, phase separation was found for the whole region of the magnetically ordered phase [15]. Since this result is based on a weak-coupling expansion, it is far from clear whether it holds for finite values of the interaction U as well. Results from a numerically exact solution of the Hubbard model in $D = \infty$ based on Quantum Monte-Carlo simulations for example showed no evidence for phase separation [16], but these calculations were done in the paramagnetic phase and at finite, comparatively high temperatures.

The question whether phase separation in the Hubbard model occurs in a certain parameter regime is of some importance for two reasons. First, from a model theoretical point of view, it is of course interesting to explore the stability of the different possible ordered phases which might be unstable with respect to phase separation. Second, a vicinity to phase separation has been discussed as one of the possible ingredients to the superconductivity in the high-T_c cuprates [17,18]. Moreover, a tendency towards phase separation together with the long-range part of the Coulomb interaction may in principle lead to charge ordered states such as stripe-phases.

Phase separation has long been predicted [17,19] and indeed been observed for the t-J model in $D = 1, 2$ (for a review see *e.g.* [20]). Since the t-J model for vanishing J is connected to the Hubbard model in the

[a] e-mail: thomas.pruschke@physik.uni-augsburg.de

limit $U/t \to \infty$ [21], additional information about phase separation in the strong coupling limit could thus be obtained. However, the early work on phase separation in the t-J model established phase separation only for $J \sim t$ [20]. Despite ongoing efforts [22] the situation in the limit $J \to 0$ is far from clear and more detailed studies are necessary. It thus appears that the question about phase separation in the Hubbard model even for $U/t \to \infty$ in $D = 2$ has not been clarified yet, since also direct inspection of the Hubbard model in the limit $U/t \to \infty$ leads to contradictory results [23,24].

The results for the $2D$ Hubbard model for finite U available so far have not revealed signs for phase separation [20,25]. However, these results are typically based on Quantum Monte-Carlo or related techniques, which have severe problems in the interesting parameter regime close to half filling and at very low temperatures. Consequently, one either has to restrict oneself to rather small system sizes [20] or use further approximations [25]. Thus, to our present knowledge a detailed study of the ground state phase diagram of the Hubbard model in the thermodynamic limit and in the vicinity of half filling, comprising weak, intermediate and strong coupling within a non-perturbative approach is not available.

Such an approach is provided by the limit $D \to \infty$, which allows for in principle exact calculations in the thermodynamic limit for all model parameters, even at $T = 0$. The price one pays is the neglect of non-local dynamics, which of course is most severe for $D \leq 2$. Nevertheless, the theory can give valuable information about whether phase separation is possible at all.

The paper is organized as follows. In Section 2, we give a brief description of the solution of the Hubbard model in the limit $D \to \infty$. Results for the phase diagram and the dynamics in the different phases are presented in Section 3. The main conclusions of the paper are summarized in Section 4.

2 Theoretical background

2.1 General remarks

The dynamical mean-field theory (DMFT) to exactly solve the Hubbard model in the limit $D \to \infty$ is based on the work by Metzner and Vollhardt [10] and is by now well-established [13]. The basic ingredient is that for $D \to \infty$ the proper single-particle self energy $\Sigma(\boldsymbol{k}, z)$ becomes purely local or momentum independent, *i.e.* $\Sigma(\boldsymbol{k}, z) \stackrel{D\to\infty}{\longrightarrow} \Sigma(z)$ [10,12]. This can be used to map the Hubbard model (1) onto an equivalent quantum impurity problem supplemented by a self-consistency condition [13]. The remaining problem (the solution of a quantum impurity model) is, however, highly nontrivial. Several approximate and numerically exact techniques are currently available [13,26].

Most of these methods cannot access $T \to 0$ or are restricted to the weak-coupling regime of the Hubbard model. The most reliable technique to solve the quantum impurity problem for all interaction strenghts U and fillings n at $T = 0$ and low T is the numerical renormalization group (NRG) [26,27]. Originally, this method was set up to treat the paramagnetic problem only [27], but recent extensions have shown that calculations with a symmetry breaking field are possible with a similar level of accuracy, too [28,29]. Hence we are able to study magnetically ordered phases directly at $T = 0$.

In contrast to the standard NRG, a more refined approach has to be used to calculate dynamical quantities in the presence of a magnetic field. This has first been noted by Hofstetter, who observed discrepancies in the magnetization calculated from the spectral functions and the ground state occupation numbers [29]. To resolve this problem, he proposed a modification of the standard method [30] to calculate the spectral function. A more detailed discussion of this technical point and its physical background will be presented elsewhere.

There are in principle two ways to determine the phase boundary between the paramagnetic and a magnetically ordered state. First, one can calculate the susceptibility corresponding to the anticipated order and look for a divergence. Second, one can allow for a proper symmetry breaking in the one-particle Green function and search for the region in parameter space where a solution with broken symmetry becomes stable. Especially for $T = 0$ the first method is rather cumbersome in general and, by construction, also makes no statement about the thermodynamic stability of phases beyond the critical point.

We thus use the second approach as our method of choice. However, this prohibits the search for incommensurate phases, because only broken symmetries with a commensurate wave vector can be implemented that way. Since we are interested mainly in standard Néel type antiferromagnetic order, the proper way is to introduce an AB-lattice structure and allow for different sublattice magnetizations. The resulting Green function then becomes a 2×2 matrix, which within the DMFT and for nearest-neighbor hopping on a simple hypercubic lattice

$$t_{ij} = \begin{cases} -t & \text{if } i,\, j \text{ are nearest neighbors} \\ 0 & \text{else} \end{cases} \tag{2}$$

has the form [13]

$$\mathsf{G}_{\boldsymbol{k}\sigma}(z) = \begin{pmatrix} z + \mu - \Sigma_\sigma^{\mathrm{A}}(z) & -\epsilon_{\boldsymbol{k}} \\ -\epsilon_{\boldsymbol{k}} & z + \mu - \Sigma_\sigma^{\mathrm{B}}(z) \end{pmatrix}^{-1}, \tag{3}$$

where $\boldsymbol{k}$ is a vector in the magnetic Brillouin zone (MBZ). For the Néel state on an AB-lattice a further simplification arises from the symmetry $\Sigma_\sigma^{\mathrm{A}}(z) = \Sigma_{\bar{\sigma}}^{\mathrm{B}}(z)$. For the calculation this means that we do not have to solve independent quantum impurity models for the two sublattices, but only one for say sublattice A.

But how to control the filling if the homogeneous solution (homogeneous concerning the charge distribution) turns out to be unstable towards phase separation? Fixing the chemical potential μ is not sufficient as the system will be driven to a filling corresponding to a stable solution, such as $n = 1$. To enforce a metastable state with

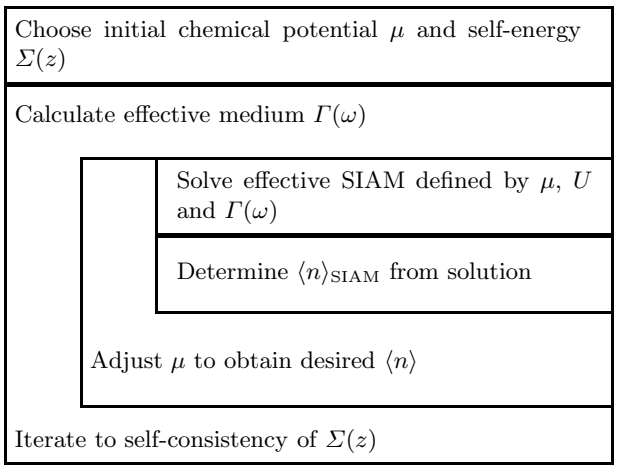

Fig. 1. Flow diagram for the DMFT self-consistency cycle with fixed filling $\langle n\rangle$.

finite doping we adopt a procedure which has been already used in calculations for the half-filled Hubbard model in a homogeneous magnetic field [31]. The schematic flow diagram of the resulting DMFT self-consistency cycle is shown in Figure 1. Starting from a paramagnetic solution for the desired doping, a homogeneous or staggered symmetry breaking is introduced and the corresponding effective medium, $\Gamma_\sigma(\omega)$, for the DMFT cycle is determined [13]. Keeping the medium $\Gamma_\sigma(\omega)$ fixed, one now varies the on-site energy of the effective SIAM until the desired doping has been reached. This result is used to obtain a new effective medium, and the procedure is repeated until convergence is reached. It should be noted that, for a metastable state, no true convergence can be reached for a finite number of iterations in the sense that the solution, when iterated further without adjusting the filling properly, will flow again into the phase separated one. Typically, for such a calculation, the on-site energy between successive DMFT iterations shows a weakly damped oscillatory behavior. We thus iterate the system until the chemical potential does not change by more than 2–3% between two successive iterations and the physically interesting quantities do not show any visible qualitative changes. At this point, in order to minimize errors, we calculate all quantities by averaging over several iterations.

To find the correct ground state, we need to calculate the ground state energy

$$\frac{E}{N} = \frac{1}{N}\langle H\rangle = \frac{1}{N}\langle H_t\rangle + \frac{U}{N}\sum_i \langle n_{i\uparrow}n_{i\downarrow}\rangle, \qquad (4)$$

where H_t is the kinetic part of the Hamiltonian (1). The expectation value $\langle n_{i\uparrow}n_{i\downarrow}\rangle$ can be determined within the NRG directly. The quantity $\langle H_t\rangle$, on the other hand, depends on the phase we are looking at. For the para- and ferromagnetic phases it is simply given by [13]

$$\frac{1}{N}\langle H_t\rangle = \sum_\sigma \int_{-\infty}^{\infty} \mathrm{d}\epsilon\ \epsilon\ \rho^{(0)}(\epsilon) \int_{-\infty}^{\infty} \mathrm{d}\omega f(\omega) A_\sigma(\epsilon,\omega), \qquad (5)$$

with $\rho^{(0)}(\epsilon)$ the density of states (DOS) for the non-interacting system, $f(\omega)$ the Fermi function and

$$A_\sigma(\epsilon,\omega) = -\frac{1}{\pi}\Im m \frac{1}{\omega+\mu-\epsilon-\Sigma_\sigma(\omega+\mathrm{i}0^+)}$$

the spectral function of the Hubbard model in the DMFT, *i.e.* with $\boldsymbol{k}$-independent one-particle self energy.

For an antiferromagnetic state with Néel order one has to take into account the AB-lattice structure and the formula becomes [13]

$$\frac{1}{N}\langle H_t\rangle = 2\int_{-\infty}^{\infty} \mathrm{d}\epsilon\ \epsilon\ \rho^{(0)}(\epsilon) \int_{-\infty}^{\infty} \mathrm{d}\omega f(\omega) B(\epsilon,\omega) \qquad (6)$$

instead, with

$$B(\epsilon,\omega) = -\frac{1}{\pi}\Im m \frac{1}{\sqrt{\zeta_\sigma(\omega)\zeta_{\bar\sigma}(\omega)}-\epsilon}$$

and $\zeta_\sigma(\omega) = \omega+\mu-\Sigma_\sigma(\omega+\mathrm{i}0^+)$. Obviously, expression (6) reduces to (5) without magnetic order, *i.e.* $\zeta_\sigma(\omega) = \zeta_{\bar\sigma}(\omega)$.

Throughout the rest of the paper we concentrate on results for a simple hypercubic lattice and nearest-neighbor hopping (2). The resulting DOS $\rho^{(0)}(\epsilon)$ then becomes [10,12]

$$\rho^{(0)}(\epsilon) = \frac{1}{t^*\sqrt{\pi}}\mathrm{e}^{-(\epsilon/t^*)^2}. \qquad (7)$$

In the following we use $t^* = 2\sqrt{D} = 1$ as our unit of energy.

2.2 Weak-coupling results

Let us briefly review some weak-coupling results as these will be frequently referred to in Section 3. Since the hypercubic lattice is a bipartite lattice, one obtains in lowest order, *i.e.* in Hartree approximation, a transition into a Néel state for any $U > 0$ at $T = 0$ below a critical doping $\delta_c^{\rm H}(U)$. For small $U \to 0$ the magnetization m as well as the critical doping depend non-analytically on U, *i.e.* $m, \delta_c^{\rm H} \propto \exp\left(-1/(U\rho^{(0)}(0))\right)/U$ independent of the dimension.

A quantity of particular interest in the DMFT is the single-particle Green function. The general structure of the Green function in the Néel phase for both Hartree theory and DMFT is given by expression (3), where in the Hartree approximation $\Sigma_\sigma(z)$ reduces to $\Sigma_\sigma^{\rm H}(z) = Un_{\bar\sigma} = \frac{1}{2}U(n-\sigma m)$ with n the filling and m the magnetization. The local Green function is obtained from (3) by summing over $\boldsymbol{k} \in$ MBZ, which yields for example for spin up

$$G_\uparrow(\omega) = \frac{\zeta_\downarrow(\omega)}{\sqrt{\zeta_\uparrow(\omega)\zeta_\downarrow(\omega)}}\ G^{(0)}\left(\sqrt{\zeta_\uparrow(\omega)\zeta_\downarrow(\omega)}\right) \qquad (8)$$

with $\zeta_\sigma(\omega) = \omega + i0^+ + \mu - \frac{U}{2}n + \sigma\frac{U}{2}m$ and

$$G^{(0)}(z) = \int_{-\infty}^{\infty} \mathrm{d}\epsilon\ \frac{\rho^{(0)}(\epsilon)}{z-\epsilon}\,. \qquad (9)$$

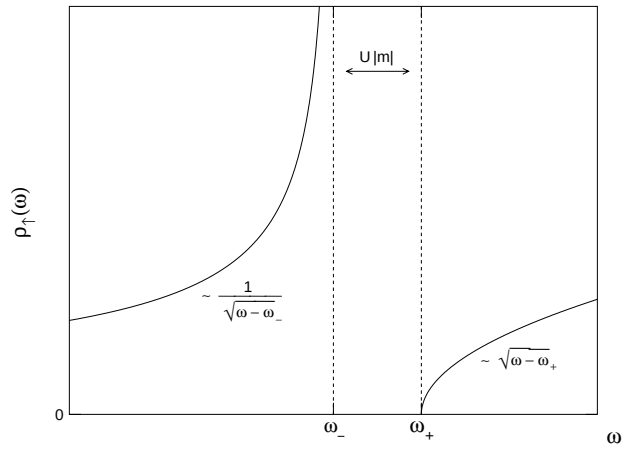

Fig. 2. Behavior of the DOS for the majority spins on a particular sublattice in Hartree approximation close to the gap edges.

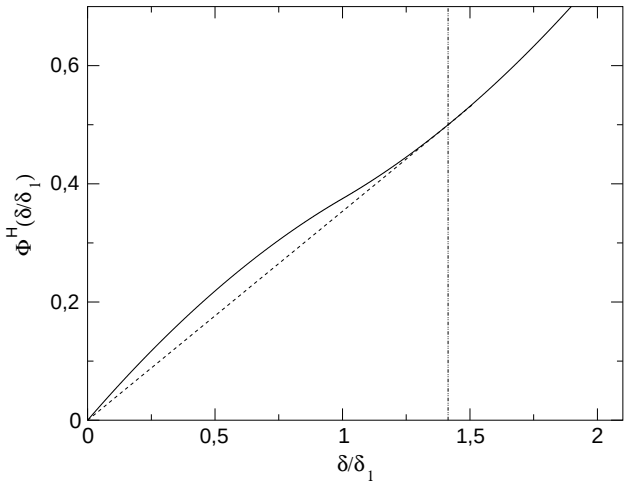

Fig. 3. The function $\Phi^{\mathrm{H}}(\delta/\delta_1)$ from equation (12). Note the concave curvature between $\delta = 0$ and $\delta = \delta_1$. The dashed line shows the actual behavior of the ground state energy following from a Maxwell construction.

For the further discussion let us define

$$\omega_- = \tfrac{U}{2}n - \mu - \tfrac{U}{2}m$$

$$\omega_+ = \tfrac{U}{2}n - \mu + \tfrac{U}{2}m.$$

Then, as long as $\omega \leq \omega_-$ or $\omega \geq \omega_+$, the radicant in (8) is positive and the resulting DOS can be expressed as

$$\rho_\uparrow(\omega) = \frac{\zeta_\downarrow(\omega)}{\sqrt{\zeta_\uparrow(\omega)\zeta_\downarrow(\omega)}}\rho^{(0)}\left(\sqrt{\zeta_\uparrow(\omega)\zeta_\downarrow(\omega)}\right).$$

For $\omega_- < \omega < \omega_+$, on the other hand, the radicant in (8) is negative, *i.e.* $\sqrt{\zeta_\uparrow(\omega)\zeta_\downarrow(\omega)} = \mathrm{i}\sqrt{|\zeta_\uparrow(\omega)\zeta_\downarrow(\omega)|}$. Since for the particle-hole symmetric DOS (7) the Green function $G^{(0)}(z)$ defined in (9) for purely imaginary arguments is purely imaginary, too, one finds

$$\rho_\uparrow(\omega) = 0,$$

i.e. the DOS has a gap between ω_- and ω_+. As one approaches ω_- from below or ω_+ from above, it is easy to confirm that

$$\rho_\uparrow(\omega) \approx \begin{cases} \sqrt{\dfrac{Um}{|\omega-\omega_-|}}\rho^{(0)}(0) & \omega \nearrow \omega_- \\ \sqrt{\dfrac{|\omega-\omega_+|}{Um}}\rho^{(0)}(0) & \omega \searrow \omega+ \end{cases}. \qquad (10)$$

The corresponding DOS for $\sigma =\downarrow$ has a similar behavior. Here, however, the DOS diverges like $1/\sqrt{|\omega-\omega_+|}$ at the upper gap edge, and vanishes like $\sqrt{|\omega-\omega_-|}$ at the lower one.

In order to determine the thermodynamically stable phase one has to calculate the ground state energy as function of the doping $\delta = 1-n$. The result up to second order in U is [15]

$$E(\delta) - E(0) = -\frac{U}{2}\delta + \alpha^{\mathrm{H}}\Phi^{\mathrm{H}}(\delta/\delta_1), \qquad (11)$$

where

$$\Phi^{\mathrm{H}}(x) = \begin{cases} \dfrac{1}{2}x\left(1-\dfrac{1}{4}x\right) & x < 1 \\ \dfrac{1}{4}\left(1+\dfrac{1}{2}x^2\right) & x > 1 \end{cases} \qquad (12)$$

and δ_1 is the critical doping for antiferromagnetism in Hartree approximation. The coefficient α^{H} is given by $\alpha^{\mathrm{H}} = 2\delta_1^2/\rho^{(0)}(0)$. The function $\Phi^{\mathrm{H}}(\delta/\delta_1)$ appearing in expression (11) leads to the full line in Figure 3. Apparently, this function is not convex for small δ, *i.e.* the resulting phase is thermodynamically unstable towards phase separation for dopings less than $\delta_c = \sqrt{2}\delta_1$. The resulting ground state energy is then obtained from a Maxwell construction, given by the straight dashed line in Figure 3.

3 Results

Let us start with a short overview of the behavior at half filling, $n = 1$. Here, the Néel phase is energetically stable. The variation of the DOS for increasing U from $U = 1$ (full curve) to $U = 6$ (dashed curve) is shown in Figure 4. As expected, the DOS for small U resembles the form (10) predicted for weak-coupling, *i.e.* one sees the remnants of the characteristic square-root divergence in the spin up DOS at the lower gap edge and a corresponding power law at the upper gap edge. These characteristic features however vanish rapidly with increasing U, and already for $U = 3$ the DOS mainly consists of the Hubbard peaks at $\omega = +U/2$ and $\omega = -U/2$ for $\sigma =\downarrow$ and $\sigma =\uparrow$, respectively; reminiscent of the behavior expected for the Mott-Hubbard insulator, where only the incoherent charge excitation peaks at high energies are present [2,13,32,33]. Note that neither from the spectra in Figure 4 nor from the behavior of the magnetic moment in the inset of Figure 4 one can infer that at $U \approx 4.1$

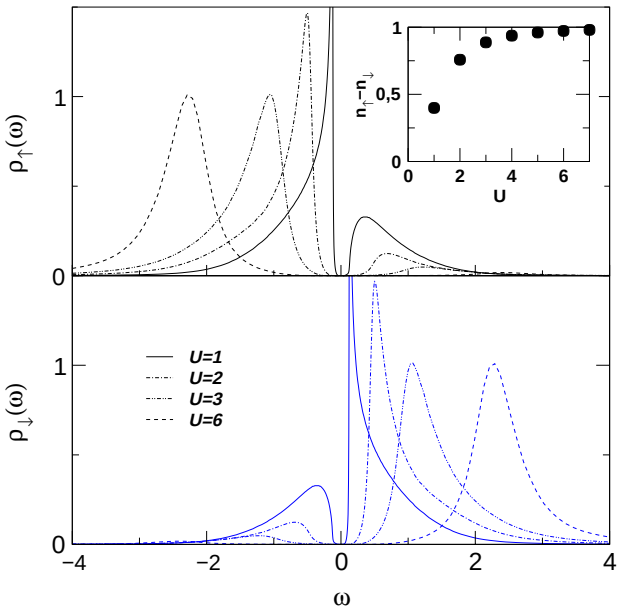

Fig. 4. DOS for spin up and down at half filling in the antiferromagnetic phase as function of U. While for small values of U the weak-coupling form (10) is approximately reproduced, the DOS for large U is basically that of the Mott-Hubbard insulator. The inset shows the magnetization as function of U.

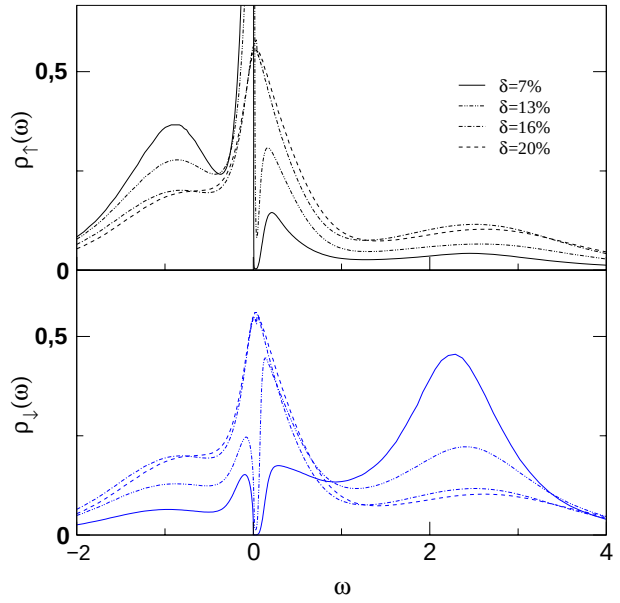

Fig. 5. DOS for spin up and down for $U = 3$ and different dopings $\delta = 7\%$, $\delta = 13\%$, $\delta = 16\%$ and $\delta = 20\%$. The system at $\delta = 20\%$ is already in the paramagnetic phase.

the Mott-Hubbard metal-insulator transition occurs in the paramagnetic state [32,33].

Keeping U fixed at $U = 3$ and increasing δ leads to the spectra shown in Figure 5. Quite interestingly, the typical weak-coupling characteristics reappear in the spectra for small doping and are still recognizable for $\delta = 13\%$. Note also that upon variation of doping and hence of the magnetization the spectra are not shifted in the same way as

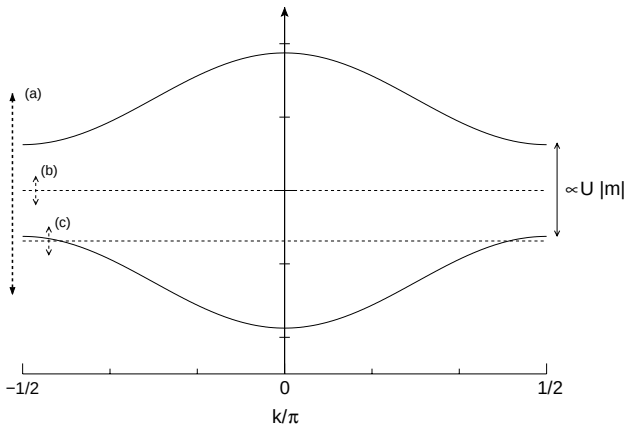

Fig. 6. Schematic picture of the Hartree bandstructure of the Hubbard model in the Néel state. The arrows at the left hand side of the figure represent the energy scales of the corresponding *paramagnetic* Fermi liquid for half filling and weak coupling (a), half filling and intermediate coupling (b) and finite doping and intermediate coupling (c).

in Hartree theory. Instead, the dominant effect is a strong redistribution of spectral weight from the Hubbard bands to the Fermi level. Eventually, in the paramagnetic phase one recovers the well-known three peak structure of the doped Hubbard model in the DMFT [13].

The evolution of the spectra both at and off half filling can be understood within a simple picture. In Figure 6 we show a sketch of the Hartree bandstructure of the Hubbard model in the Néel state, which has two branches in the MBZ and a gap of width $\propto U|m|$ between them. If, on the other hand, we inspect the *paramagnetic* solution, one for example finds at half filling and for small values of U a Fermi liquid with quasiparticles defined on an energy scale larger than $U|m|$. This situation is indicated by the arrow labeled (a) on the left side of Figure 6. Here we expect, and indeed find for the antiferromagnetic solution (see full curve in Fig. 4), a DOS that shows the characteristic van-Hove singularities of Figure 2. Increasing U eventually leads to a situation, where the energy scale for the quasiparticles in the paramagnetic state is finite but much smaller than $U|m|$ (arrow (b) in Fig. 6). The self-energy in the energy region of the van-Hove singularities then has a large imaginary part and will completely smear out the characteristic structures. Further increasing U into the Mott-Hubbard insulator will then not change the picture qualitatively, explaining the similarity between the curves for $U = 3 < U_{\mathrm{MIT}}$ and $U = 6 > U_{\mathrm{MIT}}$ in Figure 4. With finite doping, we move the chemical potential into, *e.g.*, the lower band; this means that even for a relatively small quasiparticle energy scale one again sees the van-Hove singularities at the band edge, which results in the well defined singularities in the spectra for small doping in Figure 5.

From the occupation numbers n_σ obtained after convergence of the DMFT calculation one can calculate the magnetization per electron, $m = (n_\uparrow - n_\downarrow)/(n_\uparrow + n_\downarrow)$, as function of the doping δ. The results for $U = 1$ and $U = 3$

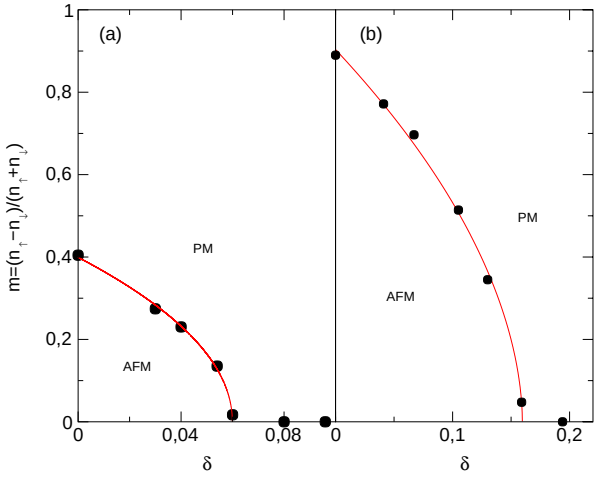

Fig. 7. Doping dependence of the magnetization per electron for $U = 1$ (a) and $U = 3$ (b). The full lines are fits with the function (13), the resulting fit parameters are summarized in Table 1.

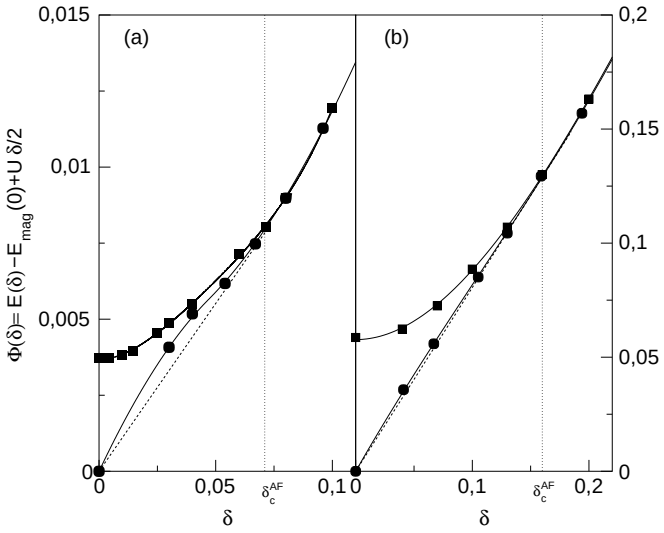

Fig. 8. Doping dependence of the energy of the paramagnetic phase (squares) and the Néel phase (circles) for $U = 1$ (a) and $U = 3$ (b). The full lines are fits with the function (14), the corresponding fit parameters are summarized in Table 1. The dashed lines are the result of a Maxwell construction for the ground state energy.

are shown in Figure 7a and b together with a fit to a power law

$$m(\delta) = m_0 \left| 1 - \frac{\delta}{\delta_c^{\mathrm{AF}}} \right|^{\nu} . \tag{13}$$

The resulting fit parameters are summarized in Table 1. As expected for a mean-field theory, the value for the critical exponent is $\nu = 1/2$.

Finally, with the converged DMFT self-energy $\Sigma_\sigma(z)$ we can calculate the expectation value $\langle H \rangle / N$ according to equations (4, 5) respectively (6) for the paramagnetic and antiferromagnetic phase. The results for the characteristic function

$$\Phi(\delta) = E(\delta) + \frac{U}{2}\delta - E_{\mathrm{mag}}(0)$$

are summarized in Figure 8a and b. In Figure 8 the energies of the antiferromagnetic phase are represented by the circles, those of the paramagnetic phase by squares. The full lines interpolating the antiferromagnetic data are fits to the function

$$\Phi(\delta) = \alpha \Phi^{\mathrm{H}}(\delta/\delta_1) + \gamma \left(\frac{\delta}{\delta_1} \right)^3 \tag{14}$$

with $\Phi^{\mathrm{H}}(x)$ according to (12). The fit parameters are summarized in Table 1. The use of the function $\Phi^{\mathrm{H}}(x)$ in (14) is motivated by the results of van Dongen [15]. The lines interpolating the paramagnetic data are meant as guides to the eye only. The dotted vertical lines denote the value δ_c^{AF} as obtained from Figure 7.

The antiferromagnet obviously has the lower energy as compared to the paramagnet in the region $0 \leq \delta \leq \delta_c^{\mathrm{AF}}$. However, in both cases $U = 1$ and $U = 3$ we find a clear non-convex behavior in $E(\delta)$ in that region, *i.e.* the aforementioned signature of an instability towards phase separation. The true ground state energy as function of δ is obtained again *via* a Maxwell construction, leading to the dashed lines in Figure 8 and the values δ_c^{PS} given in Table 1. Note that in both cases $\delta_c^{\mathrm{AF}} \approx \delta_c^{\mathrm{PS}}$ within the accuracy of the fitting procedure.

Table 1. Results of the fits of $m(\delta)$ in Figure 7 to expression (13) and $E(\delta)$ in Figure 8 to (14).

	Magnetization			Energy			
U	m_0	δ_c^{AF}	ν	δ_c^{PS}	δ_1	$\alpha/\alpha^{\mathrm{H}}$	γ
1	0.4	0.06	0.49	0.07	0.047	0.52	0
3	0.9	0.16	0.54	0.157	0.191	0.33	0.026

While for $U = 1$ the function $\Phi(\delta)$ nicely follows the weak-coupling prediction (11) with renormalized constant α one finds a sizeable contribution $\sim\delta^3$ for $U = 3$. This additional term results in a much weaker non-convex behavior of $E(\delta)$ for $U = 3$.

For values $U > 4$ we were not able to find a stable solution with Néel order and well-defined doping $\delta > 0$, although for $\delta < \delta_c(U)$ the paramagnetic phase becomes unstable. However, the numerical calculations rather produce a cycle encompassing a range of fillings instead of one solution with definite filling here. It might be interesting to note that at least each of the fillings in this cycle has a unique magnetization associated with it and that all spectra in this cycle correspond to an insulator. Currently it is neither clear what type of magnetic solution we find here, nor whether the breakdown of the Néel solution is a true physical effect or due to numerical problems. Since at half filling the Néel state is present at these values of U, incommensurate structures or again a phase separated state seem to be possible.

For values of U beyond $U_c \approx 25$ yet another magnetic phase appears, namely the ferromagnet. The existence of

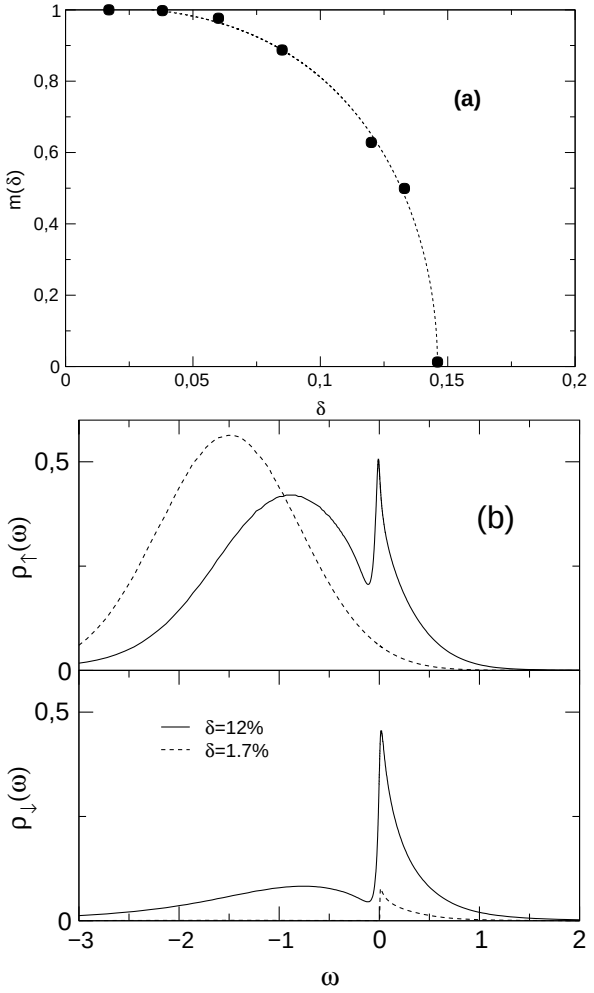

Fig. 9. (a) Ferromagnetic magnetization *per electron* as function of doping δ for $U = 50$. The full line is a fit to the function (15). The critical doping is $\delta_c \approx 14.6\%$. Note that for $\delta \to 0$ the results are consistent with a fully polarized ferromagnetic state. (b) Local density of states for $U = 50$ and two characteristic dopings $\delta = 12\%$ (full lines) and $\delta = 1.7\%$ (dashed lines). In contrast to the Stoner theory, one finds comparatively small shifts in the spectra, but a strong redistribution of spectral weight.

this phase has been observed in the case of a hypercubic lattice and $U = \infty$ [34] and for a generalized fcc lattice [35] before. Since these calculations had to be done at finite and comparatively high temperatures, questions regarding the ground state magnetization and, especially in the case of a hypercubic lattice, the actual extent of the ferromagnetic phase in (δ, U) space could not be discussed satisfactorily.

As an example for the ferromagnetic phase at $T = 0$ Figure 9 shows the magnetization per electron, $m(\delta) = (n_\uparrow - n_\downarrow)/(n_\uparrow + n_\downarrow)$ as function of doping (Fig. 9a) and the local DOS for two dopings (Fig. 9b) ($U = 50$). The data for $m(\delta)$ in Figure 9a are fitted to the function

$$m(\delta) = m_0 \sqrt{1 - \left(\frac{\delta}{\delta_c}\right)^{\nu}}, \tag{15}$$

and the result is given by the dotted line. The parameters for the fit are $m_0 = 1$, $\delta_c = 14.6\%$ and $\nu = 2.75$. While for $\delta \nearrow \delta_c$ the typical mean-field behavior, *i.e.* $m(\delta) \propto \sqrt{1 - \frac{\delta}{\delta_c}}$, is obtained, the result for $\delta \to 0$ is rather unconventional, *viz.* $m(\delta) \propto 1 - \frac{1}{2}\left(\frac{\delta}{\delta_c}\right)^{2.75}$. This fit assumes that a fully polarized state is only reached as $\delta \to 0$ [36]. Note, however, that the numerical results for the magnetization $m(\delta)$ for small δ are also consistent with a fully polarized ferromagnet at finite δ.

It is also quite apparent from the DOS in Figure 9b, that the ferromagnetism found here cannot be understood on the basis of the typical Stoner theory. In contrast to the shifts of the spectrum expected in the latter, we observe a strong redistribution of spectral weight instead, but retain otherwise the typical structures due to the strong correlations. Only in the case $\delta \to 0$ the spectrum again resembles that of a free system for the (almost completely polarized) majority spins. The minority spins become strongly depleted below the Fermi energy, the spectral weight can be found almost completely in the upper Hubbard band situated around $\omega \approx U/2$ (not shown in the figure). Nevertheless, we observe a tiny resonance *just above* the Fermi energy even as $\delta \to 0$.

4 Summary and conclusion

In this paper, we used the dynamical mean-field theory together with Wilson's numerical renormalization group to investigate the ground-state properties of the Hubbard model on a hypercubic lattice with nearest-neighbor hopping both at and off half-filling. While at half-filling the ground-state is antiferromagnetic for all $U > 0$, at least for the weak and intermediate coupling regime this magnetic order can only be realized in a phase-separated state for any finite doping, thus supporting and extending earlier weak-coupling predictions.

The mapping of the Hubbard model for large U to an antiferromagnetic t-J model strongly suggests the dominance of antiferromagnetism in the ground state. The results for the Hubbard model in this paper show, however, that the type of magnetic order for intermediate values of the Coulomb repulsion U off half filling is still an open issue; furthermore, the role of phase-separation (which is observed for $U \leq 3$) has still to be clarified for larger values of U.

The results are summarized in the schematic (δ, U) ground state phase diagram of Figure 10. To allow the inclusion of all values $0 \leq U < \infty$, the ratio $U/(1+U)$ is used on the abcissa. Close to half filling we find a phase separated Néel antiferromagnet up to a certain value of $U < 4$. The magnetization as function of doping follows a typical mean-field behavior in all cases studied and the spectra

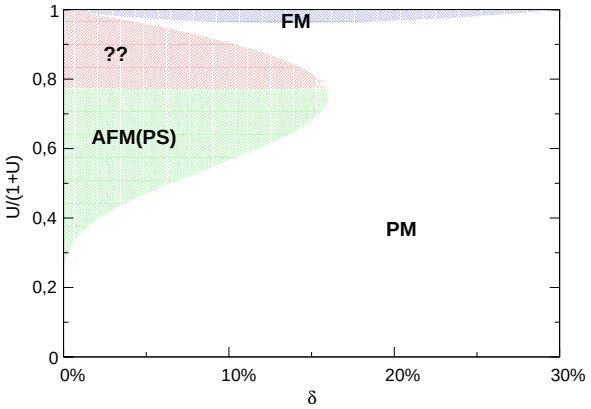

Fig. 10. Schematic ground state phase diagram. At half-filling ($\delta = 0$), the ground state is antiferromagnetic. Close to half filling and small U, a phase separated antiferromagnet is realized. For values of U beyond $U \approx 4$ a magnetic phase is observed, whose precise character could however not be identified. For very large $U > 25$ and up to $\delta \approx 30\%$ a ferromagnet is found.

show the characteristic van-Hove singularities of the band structure in the Néel state in cases where the characteristic energy scale of the paramagnet is large enough. Most important is the observation that, as typical for correlated ordered systems, the spectra are not strongly shifted, as *e.g.* predicted by Hartree theory, but rather show a strong redistribution of spectral weight.

For values of $U > 4$ the system shows the tendency towards a magnetic instability, which could not be further identified due to technical problems in the solution of the DMFT self-consistency. However, we at least can exclude ferromagnetism here and a speculative possibility would be the occurence of incommensurate phases or magnetic phases with additional charge order. While the former cannot be addressed easily within the present method, the latter possibility will be investigated further.

At very large values of $U > 25$, there is a region of ferromagnetism, extending between $0 < \delta < 30\%$ as $U \to \infty$ [34]. For a fixed value of U, the magnetization per electron in the ferromagnetic state shows the tendency to saturate near half filling; from the numerical data it is of course impossible to reliably conclude whether the system is fully polarized at a finite δ already or only as $\delta \to 0$. The data are consistent with both scenarios, but the latter is supported by analytical treatments of the case $\delta \to 0$. As in the case of the antiferromagnet, the spectrum shows a rather strong redistribution of spectral weight, not simply a shift of the features, as would be expected from Stoner theory.

The phase diagram shows a peculiarity, which has alread been pointed out by Obermeier *et al.* [34]. In the region of very large U and $\delta \to 0$ there exists the possibility of a direct transition between the "antiferromagnetic" phase and the ferromagnet. As at the point $(\delta, U) = (0, \infty)$ all possible spin configurations are degenerate, one can speculate how the phase diagram looks like as $(\delta, U) \to (0, \infty)$ [37]. Generic possibilities are sketched in Figure 11. There can either be a direct transition between the two phases (Fig. 11a), which quite likely would then be of first order, a gap filled by a paramagnetic phase (Fig. 11b) or a new phase, *e.g.* a ferrimagnet interpolating between the two extremes. The a priori exclusion or verification of any of these structures is, without a detailed knowledge of the analytic behaviour of the relevant quantities as function of (δ, U) in the vicinity of $(\delta, U) = (0, \infty)$, not possible.

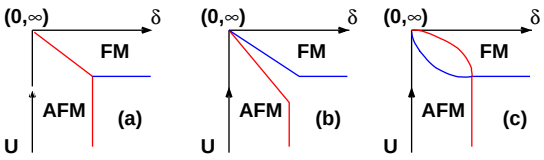

Fig. 11. Possible realizations of the phase diagram as $(\delta, U) \to (0, \infty)$: A direct transition between an antiferromagnet and a ferromagnet as in (a), a small paramagnetic phase between the two as in (b) or a mixed type of phase (*e.g.* ferrimagnet) as in (c).

While there is a consensus about the magnetic properties of the Hubbard model in a qualitative sense, the direct inspection of details still reveals unexpected surprises. Even within the DMFT, where one can safely state that the paramagnetic phase diagram including the Mott-Hubbard metal insulator transition is now understood, the investigation of the magnetic properties is far from complete. Obvious open questions are the magnetic properties at intermediate values of U and the behavior when the antiferromagnetic and ferromagnetic phases meet. Furthermore, the behaviour of the magnetic phases, especially the spectral properties in the ordered phases, in the presence of a frustration due to longer range hopping, has not been addressed yet. This might be of some interest regarding the question how the first order Mott-Hubbard transition manifests itself in the magnetically ordered state. Work along these lines is in progress.

We acknowledge useful discussions with P.G.J. van Dongen, M. Jarrell, J. Keller, D. Logan, M. Vojta and D. Vollhardt. This work was in part supported by the SFB 484 *Kooperative Phänomene im Festkörper* and the Leibniz Computer center.

References

1. J. Hubbard, Proc. R. Soc. London A **276**, 238 (1963); M.C. Gutzwiller, Phys. Rev. Lett. **10**, 59 (1963); J. Kanamori, Prog. Theor. Phys. **30**, 275 (1963)
2. See the original work in [1] and N.F. Mott, Rev. Mod. Phys. **40**, 677 (1968); W.F. Brinkman, T.M. Rice, Phys. Rev. B **2**, 4302 (1970)
3. P.W. Anderson, Solid State Phys. **14**, 99 (1963); M. Cyrot, Physica B **91**, 141 (1977)
4. H. Tasaki, Prog. Theor. Phys. **99**, 489 (1998)
5. H.J. Schulz, Phys. Rev. Lett. **64**, 1445 (1990)
6. P.W. Anderson, Science **235**, 1196 (1987); P.A. Lee, N. Nagaosa, Phys. Rev. B **46**, 5621 (1992)
7. *The Hubbard Model*, A Reprint Volume, edited by A. Montorsi (World Scientific Publ., Singapore 1992)

8. E.H. Lieb, *The Hubbard model – Some Rigorous Results and Open Problems*, *Proceedings of the XIth International Congress of Mathemantical Physics, Paris 1994*, edited by D. Iagolnitzer (International Press, 1995), p. 392; H. Tasaki, J. Phys. Cond. Matt. **10**, 4353 (1998).
9. Y. Nagaoka, Phys. Rev. **147**, 392 (1966)
10. W. Metzner, D. Vollhardt, Phys. Rev. Lett. **62**, 324 (1989)
11. A. Georges, G. Kotliar, Phys. Rev. B **45**, 6479 (1992); M. Jarrell, Phys. Rev. Lett. **69**, 168 (1992)
12. E. Müller-Hartmann, Z. Phys. B **76**, 211 (1989)
13. T. Pruschke, M. Jarrell, J.K. Freericks, Adv. Phys. **42**, 187 (1995); A. Georges, G. Kotliar, W. Krauth, M.J. Rozenberg, Rev. Mod. Phys. **68**, 13 (1996)
14. P.G.J. van Dongen, Phys. Rev. Lett. **67**, 757 (1991); Phys. Rev. B **50**, 14016 (1994)
15. P.G.J. van Dongen, Phys. Rev. B **54**, 1584 (1996).
16. J.K. Freericks, M. Jarrell, Phys. Rev. Lett. **74**, 186 (1995)
17. V.J. Emery, S. Kivelson, Physica C **209**, 597 (1993)
18. C. Castellani, C. Di Castro, M. Grilli, Phys. Rev. Lett. **75**, 4650 (1995)
19. V.J. Emery, S.A. Kivelson, H.Q. Lin, Phys. Rev. Lett. **64**, 475 (1990)
20. E. Dagotto, Rev. Mod. Phys. **66**, 763 (1994)
21. P. Fulde, *Electron correlations in molecules and solids* (Springer, Berlin 1995)
22. C.S. Hellberg, E. Manousakis, Phys. Rev. Lett. **78**, 4609 (1997); L.P. Pryadko, S. Kivelson, D.W. Hone, Phys. Rev. Lett. **80**, 5651 (1998); E. Eisenberg, R. Berkovits, D.A. Huse, B.L. Altshuler, `cond-mat/0108523` (2001)
23. G. Su, Phys. Rev. B **54**, R8281 (1996)
24. A. Tandon, Z. Wang, G. Kotliar, Phys. Rev. Lett. **83**, 2046 (1999)
25. F. Becca, M. Capone, S. Sorella, Phys. Rev. B **62**, 12700 (2000)
26. R. Bulla, A.C. Hewson, Th. Pruschke, J. Phys. Cond. Matt. **10**, 8365 (1998)
27. K.G. Wilson, Rev. Mod. Phys. **47**, 773 (1975); H.R. Krishna-murthy, J.W. Wilkins, K.G. Wilson, Phys. Rev. B **21**, 1003 and 1044 (1980)
28. T.A. Costi, Phys. Rev. Lett. **85**, 1504 (2000)
29. W. Hofstetter, Phys. Rev. Lett. **85**, 1508 (2000)
30. O. Sakai, Y. Shimizu, T. Kasuya, J. Phys. Soc. Jpn **58**, 3666 (1989)
31. L. Laloux, A. Georges, W. Krauth, Phys. Rev. B **50**, 3092 (1994)
32. Th. Pruschke, D.L. Cox, M. Jarrell, Phys. Rev. **47**, 3553 (1993)
33. R. Bulla, Phys. Rev. Lett. **83**, 136 (1999)
34. Th. Obermeier, Th. Pruschke, J. Keller, Phys. Rev. B **56**, R8479 (1997)
35. D. Vollhardt, N. Blümer, K. Held, M. Kollar, J. Schlipf, M. Ulmke, Z. Phys. B **103**, 283 (1997); M. Ulmke, Eur. Phys. J. B **1**, 301 (1998)
36. P. Fazekas, E. Müller-Hartmann, Z. Phys. B **78**, 69 (1990); G.S. Uhrig, Phys. Rev. Lett. **77**, 3629 (1996)
37. D. Vollhardt, private communication; M. Vojta, private communication